The Astrophysical Journal Letters, 885:L35 (6pp), 2019 November 10 https://doi.org/10.3847/2041-8213/ab4fed

Dark Matter Signatures of Supermassive Black Hole Binaries

Smadar Naoz[1,2], Joseph Silk[3,4,5], and Jeremy D. Schnittman[6,7]
[1] Department of Physics and Astronomy, University of California, Los Angeles, CA 90095, USA
[2] Mani L. Bhaumik Institute for Theoretical Physics, University of California, Los Angeles, CA 90095, USA
[3] Institut d'Astrophysique de Paris, UMR 7095 CNRS, Sorbonne Universités, 98 bis, boulevard Arago, F-75014, Paris, France
[4] The Johns Hopkins University, Department of Physics and Astronomy, Baltimore, MD 21218, USA
[5] Beecroft Institute of Particle Astrophysics and Cosmology, University of Oxford, Oxford OX1 3RH, UK
[6] NASA Goddard Space Flight Center, Greenbelt, MD 20771, USA
[7] Maryland Joint Space-Science Institute, College Park, MD 20742, USA
Received 2019 September 20; revised 2019 October 17; accepted 2019 October 19; published 2019 November 6

Abstract

A natural consequence of the galaxy formation paradigm is the existence of supermassive black hole (SMBH) binaries. Gravitational perturbations from a far-away SMBH companion can induce high orbital eccentricities on dark matter (DM) particles orbiting the primary SMBH via the eccentric Kozai–Lidov mechanism. This process yields an influx of DM particles into the primary SMBH ergosphere, where test particles linger for long timescales. This influx results in high self-gravitating densities, forming a DM clump that is extremely close to the SMBH. In such a situation, the gravitational-wave (GW) emission between the dark matter clump and the SMBH is potentially detectable by *LISA*. If dark matter self-annihilates, the high densities of the clump will result in a unique codetection of GW emission and high-energy electromagnetic signatures.

Unified Astronomy Thesaurus concepts: Black hole physics (159); Dark matter (353); Supermassive black holes (1663); Double quasars (406); Galaxy nuclei (609)

1. Introduction

The hierarchical nature of the galaxy formation paradigm suggests that major galaxy mergers may result in the formation of supermassive black hole (SMBH) binaries (Di Matteo et al. 2005; Hopkins et al. 2006; Robertson et al. 2006; Callegari et al. 2009). While observations of SMBH binaries are challenging, there are several observed binary precursors with sub-parsec to tens to hundreds of parsec separations (e.g., Sillanpaa et al. 1988; Rodriguez et al. 2006; Komossa et al. 2008; Bogdanović et al. 2009; Boroson & Lauer 2009; Dotti et al. 2009; Deane et al. 2014; Liu et al. 2016; Bansal et al. 2017; Kharb et al. 2017; Runnoe et al. 2017; Pesce et al. 2018; Guo et al. 2019). Furthermore, several observations of active galactic nuclei pairs with kiloparsec-scale separations have been suggested as SMBH binary precursors (e.g., Komossa et al. 2003; Bianchi et al. 2008; Comerford et al. 2009; Green et al. 2010; Liu et al. 2010; Smith et al. 2010; Comerford et al. 2018). Numerical simulations for spheroidal gas-poor galaxies suggest that these binaries can reach parsec separation and may stall there (e.g., Begelman et al. 1980; Milosavljević & Merritt 2001; Yu 2002).

While the dark matter (DM) distribution in galaxies has been studied extensively in the literature, the DM profile for sub-kiloparsec scales is largely unknown. In Naoz & Silk (2014), we suggested that gravitational perturbations in SMBH binaries can have important implications for the DM distribution around the *less* massive member of the binary. The requirement that the perturbing SMBH will be more massive than the primary arises from the need to overcome general relativistic precession of the DM particle orbits (Naoz et al. 2013). Gravitational perturbations from a far-away SMBH, on a DM particle orbiting around the primary SMBH, can result in extremely high eccentricities due to a physical process known as the "eccentric Kozai–Lidov" (EKL) mechanism (Naoz 2016). The eccentricities can reach extreme values (Li et al. 2014b) such that the pericenter passage of the DM particle reaches the SMBH ergosphere (or even the event horizon; Naoz & Silk 2014). This process results in a DM torus-like configuration around the less massive SMBH (Naoz & Silk 2014). These torus particles were initially in a less favorable EKL regime of the parameter space, compared to those that reached high eccentricities.

The low-energy, low angular momentum orbit of a test particle around a spinning black hole has been addressed in the literature up to fourth order in the post-Newtonian approximation (Will & Maitra 2017), and may yield an increase of the DM density around a rotating SMBH (Ferrer et al. 2017). The EKL mechanism in SMBH binary systems results in extremely low angular momentum orbits of the DM particles (Naoz & Silk 2014). These particles spend a significant part of their orbit zooming around the ergosphere, before continuing with their orbit (e.g., Schnittman 2015, and see below for more details).

Here we show that even the temporary accumulation of DM in the ergosphere of an SMBH, as a result of zoom–whirl orbits, can reach such high densities as to allow for formation of self-gravitating DM clumps. Such a clump then emits gravitational waves (GWs), potentially detectable by the *Laser Interferometer Space Antenna* (*LISA*), while possibly undergoing self-annihilation. This process may yield a unique cosignal of GW emission and high-energy electromagnetic signature arising from the self-annihilation process of DM (see Figure 1).

2. Self-gravitating DM Clumps

DM is expected to be inhomogeneous and clumpy (e.g., Silk & Stebbins 1993; Berezinsky et al. 2010, 2014). This clumpy nature can be explained as a simple extrapolation to very small scales of the primordial power spectrum, and in large parts of the universe these clumps are expected to be free from gas (e.g., Naoz & Narayan 2014; Popa et al. 2016; Chiou et al.

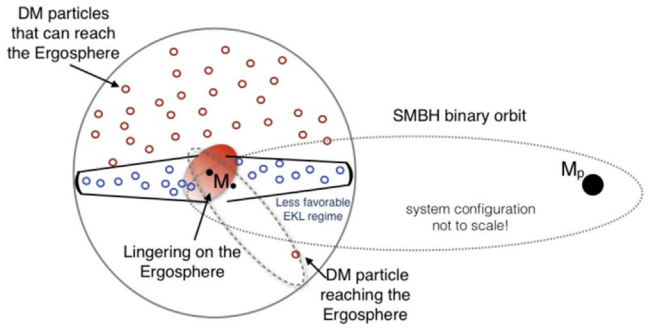

Figure 1. Illustration of the configuration. The SMBH spin can have an arbitrary orientation.

2018, 2019). Furthermore, some DM clumps may have formed shortly after or during radiation-matter equality due to phase transitions, topological defects, or collapse into primordial perturbations (e.g., Starobinskij 1992; Kolb & Tkachev 1994; Berezinsky et al. 2010). Moreover, these clumps may have formed at earlier epochs due to accretion onto primordial black holes (e.g., Bertschinger 1985; Ricotti 2009; Lacki & Beacom 2010; Eroshenko 2016; Ali-Hamoud & Kamionkowski 2017). Regardless of their formation mechanism, these clumps need to be self-gravitating in order to resist disruption from other objects in the universe.

In the vicinity of an SMBH with mass $M_\bullet$, we define the tidal radius, at which the gravitational tidal field of the SMBH overcomes the DM clump self-gravity[8]:

$$R_t \sim \left(\frac{3M_\bullet}{4\pi\rho_{\rm cl}}\right)^{1/3}, \tag{1}$$

where $\rho_{\rm cl}$ is the density of the DM clump. In Naoz & Silk (2014), we showed that gravitational perturbations from a distant SMBH can cause high-eccentricity excitations to the DM particle orbits reaching all the way to the ergosphere radius. The ergosphere represents a special location for a spinning SMBH. Here, test particles, such as DM, cannot stay stationary with respect to an outside observer (Misner et al. 1973), and tend to linger for long timescales (Schnittman 2015). We note that the analysis of this section is agnostic to any mechanism that produces an overdensity at the ergosphere and simply describes the requirement for such a clump to exist.

The ergosphere radius is (depicted in Figure 2)

$$R_{\rm min} = \frac{2GM_\bullet}{c^2}, \tag{2}$$

where c is the speed of light and G is the gravitational constant. We find the critical density for a self-gravitating clump to remain bound at the ergosphere by setting $R_{\rm min} = R_t$. In other words,

$$\rho_{\rm SG} = \frac{3}{32\pi}\frac{c^6}{G^3M_\bullet^2}. \tag{3}$$

This critical density is depicted in Figure 2.

DM self-annihilations place an upper limit on the DM density of a clump by requiring that the clump does not self-annihilate within a given time t. In other words,

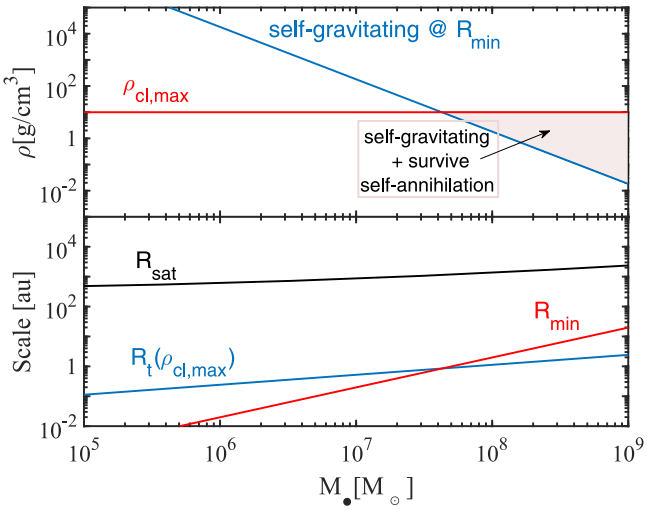

Figure 2. Typical density and physical scales in the system. Top panel: we consider the self-gravitating density required at $R_{\rm min}$ (blue line). We also show (red, horizontal line) the maximum clump density for a self-gravitating, self-annihilating DM clump within a dynamical timescale (adopting $m_\chi = 100$ Gev DM particle). Bottom panel: relevant physical scales in the system. We consider the ergosphere scale, $R_{\rm min}$ (Equation (2)), as well as the tidal radius, R_t, (Equation (1)), for $\rho_{\rm cl} = \rho_{\rm cl,max}$. We also show $R_{\rm sat}$, the saturated radius of the DM density, due to self-annihilation; see Section 3.

$$\rho_{\rm cl} \sim \frac{m_\chi}{\langle\sigma v\rangle t}, \tag{4}$$

where $\langle\sigma v\rangle$ is the thermal velocity-averaged annihilation cross-section times the particle velocity and m_χ is the mass of the DM particle. Considering the DM distribution in galaxies, the relevant timescale is typically the age of the system, which results in a saturated core density, $\rho_{\rm sat}$, at the center of a galaxy (Gondolo & Silk 1999; Lacroix et al. 2014; Lacroix & Silk 2018). Here, however, we adopt the dynamical timescale, t_D, of the self-gravitating clump (Ali-Haïmoud et al. 2016) that describes a significant change to the clump due to its own gravity:

$$t_D = \sqrt{\frac{3}{4\pi G\rho_{\rm cl}}}. \tag{5}$$

We note that the Hubble timescale is irrelevant here, because there is no need to require that the clump, or the binary, will survive for a Hubble time. Thus, setting the time in Equation (4) to be the above dynamical time, we can obtain an upper limit on the clump's density, for self-annihilating, self-gravitating clumps:

$$\rho_{\rm cl,max} \sim \frac{4\pi G}{3}\left(\frac{m_\chi}{\langle\sigma v\rangle}\right)^2. \tag{6}$$

In Figure 2, we show this upper limit for $m_\chi = 100$ Gev DM particles and adopting the canonical velocity-averaged annihilation cross-section times velocity $\langle\sigma v\rangle = 3\times10^{-26}\,{\rm cm^3\ s^{-1}}$ (Jungman et al. 1996).

From the comparison between $\rho_{\rm SG}$ and $\rho_{\rm cl,max}$, we find a minimum SMBH mass that can allow formation of a self-

[8] New work by Gafton & Rosswog (2019) showed that the radius of marginal disruption (R_t) does not change much under Kerr geometry.

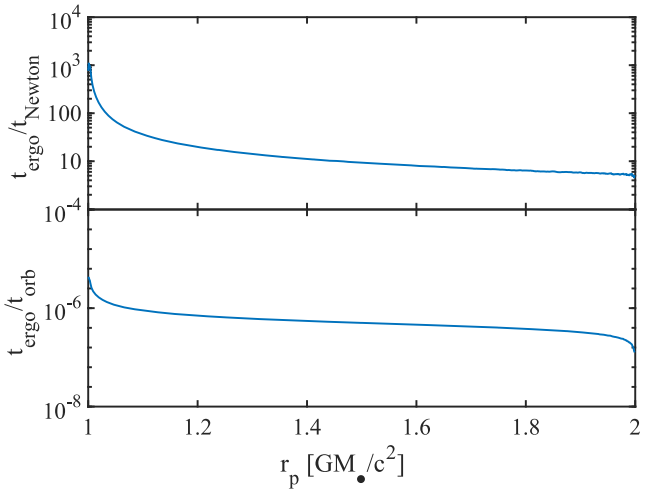

Figure 3. Top panel: we show the fractional orbital time a particle spends whirling in the ergosphere compared to the Newtonian time, $t_{\rm ergo}/t_{\rm Newton}$, as a function of the closest approach, $r_{\rm p}$, in terms of $G\,M_\bullet/c^2$. Bottom panel: we show the relative time during the orbit the particle spends in the ergosphere, $t_{\rm ergo}/t_{\rm orb}$. In this estimate, the particles were placed initially at about $40{,}000 \times GM_\bullet/c^2$, which corresponds to the average location of the particles for a $10^7\,M_\odot$ primary with a $10^9\,M_\odot$ perturber from the Naoz & Silk (2014) simulations.

gravitating spherical clump:

$$M_{\bullet,\rm lim} \sim \frac{3}{8\sqrt{2}\,\pi}\frac{c^3}{G^2}\frac{\langle\sigma v\rangle}{m_\chi}. \quad (7)$$

For $m_\chi = 100\,$Gev DM particles, we find $M_{\bullet,\rm lim} \sim 4.3 \times 10^7\,M_\odot$. This is the mass at the crossing point between $\rho_{\rm SG}$ and $\rho_{\rm cl,max}$, depicted in Figure 2. Larger DM mass particles will result in smaller limiting masses.

3. Clump Masses and Annihilation of DM

Test particles, such as DM particles, on eccentric orbits that plunge into the ergosphere, whirl around in the ergosphere a few times, then travel back out to apocenter (coined "zoom–whirl" orbits, because it involves several revolutions around the pericenter; Glampedakis & Kennefick 2002; Healy et al. 2009; Tsupko 2014). This behavior, of long-lived stable orbits, results in a density peak of DM inside $4G/c^2$ (as shown numerically by Schnittman 2015). In Figure 3, we show the fraction of the orbit that a particle will spend zooming in the ergosphere compared to the Newtonian orbit (top) and as a function of the total orbit (bottom).

To calculate the time spent in the ergosphere (Figure 3), we launch test particles on highly eccentric orbits with apocenter at $r = 40{,}000M$, and pericenter ranging from $r = 1M$ (the horizon) out to $r = 2M$ (the outer surface of the ergosphere), where $M = G\,M_\bullet/c^2$. Along these Kerr geodesic trajectories, we simply integrate the coordinate time spent inside the ergosphere for each particle, and compare that to the total coordinate time of the orbit, and also the amount of time that would be spent inside of $r = 2M$ with a Newtonian, nonrelativistic orbit. From these, we see that the frame-dragging effects of the Kerr black hole lead to longer dwell times very close to the black hole, roughly a factor of ~10–1000 times longer than a Newtonian orbit.

We note that in EKL systems, such as the one considered here, gravitational perturbations from the far-away companion excite the DM particle eccentricity to extreme values, for large range of inclinations and other orbital parameters (Li et al. 2014a, 2014b; Naoz & Silk 2014). The eccentricity of these test particles continues to increase until they reach the horizon, and thus they pass through the entire ergosphere. Thus, Figure 3 depicts a typical behavior for particles that eventually will reach the ergosphere.

Naoz & Silk (2014) pointed out that DM particles can reach extreme eccentricity, from grazing the ergosphere's outer surface all the way in to the inner surface of the ergosphere. These high-eccentricity orbits result from the gravitational perturbations from a companion that is far away from the primary SMBH, via the aforementioned EKL mechanism. The system is scalable and was shown to consistently result in nearly radial orbits (e.g., Naoz et al. 2012; Li et al. 2014b, 2015). We note that even with systems for which the secular, double-averaged method[9] breaks down, even larger eccentricities are expected (e.g., Katz & Dong 2012; Antognini et al. 2014; Luo et al. 2016; Hamers 2018). Since the evolution is gradual, particles have their pericenters evolve from the outer to the inner surface of the ergosphere. In other words, at any given time particles uniformly occupy the full extent of the ergosphere.

DM particles around an SMBH are on a stable orbit as long as $\epsilon = a_{\rm DM}e_{\rm p}/(a_{\rm p}(1-e_{\rm p}^2)) < 0.1$ (Naoz 2016), where $a_{\rm DM}$ is the DM particle semimajor axis around $M_\bullet$, and $a_{\rm p}$ and $e_{\rm p}$ are the semimajor axis and the eccentricity of the perturber SMBH, respectively. An eccentric SMBH perturber with $M_{\rm p} > M_\bullet$ will excite the eccentricity of DM particles that are around $M_\bullet$ (Naoz & Silk 2014). As a proof of concept, we set $a_{\rm p}$ to be roughly the sphere of influence, thus allowing for long-term surviving SMBH binaries. The shortest EKL timescale at which particles can reach $R_{\rm min}$ is proportional to (Naoz 2016)

$$t_{\rm EKL,min} \sim \sqrt{\frac{a_{\rm p}^3}{M_{\rm p}G}}\sqrt{\frac{M_\bullet}{M_{\rm p}}}\left(\frac{e_{\rm p}}{\epsilon}\right)^{3/2} \sim 10^3\,{\rm yr}\left(\frac{a_{\rm p}}{1\,{\rm pc}}\right)^{3/2} \times \left(\frac{10^9 M_\odot}{M_{\rm p}}\right)\left(\frac{M_\bullet}{10^7 M_\odot}\right)^{1/2}\left(\frac{0.1}{\epsilon}\right)^{3/2}\left(\frac{e_{\rm p}}{0.8}\right)^{3/2}. \quad (8)$$

DM particles develop large eccentricities as time goes by until they reach such high eccentricities that they are consumed by the SMBH. We can thus scale Naoz & Silk's (2014) nominal simulations, and estimate the timescale at which ergosphere pericenter passages are expected. The timescale has a similar time dependency for different SMBH mass primaries using the scaling relation in Equation (8). We adopt this proof-of-concept time dependence for an assumed DM distribution within the SMBH sphere of influence.

To estimate the mass that is temporarily accumulated on the ergosphere as a function of time we begin by calculating the DM density around the SMBH. Gondolo & Silk (1999) showed that the distribution of DM can be enhanced around the centers of galaxies, at a radius that is at the order of the SMBH sphere of influence. We adopt the DM density profile inward of the

[9] The double-averaged method averages over each of the orbits, and thus effectively the three-body system is reduced to two orbits, interacting with each other (see for more details Naoz 2016).

sphere of influence:

$$\rho_{\rm DM}=\begin{cases}0 & r\leqslant 2GM_\bullet/c^2,\\ \rho_{\rm sat} & 2GM_\bullet/c^2<r\leqslant R_{\rm sat},\\ \rho_{\rm sat}\left(\frac{r}{R_{\rm sat}}\right)^{-\gamma} & R_{\rm sat}<r\leqslant R_{\rm spike},\end{cases} \quad (9)$$

where we assume a Navarro–Frenk–White (NFW) profile (Navarro et al. 1996) for $r > R_{\rm spike}$, and $R_{\rm spike}$, the radius at which DM density spikes, is equal to the sphere of influence. The latter can be then computed for different SMBH masses via the m–σ relation[10] (Tremaine et al. 2002). From Equation (4), the saturated density is $\rho_{\rm sat}=m_\chi/(\langle\sigma v\rangle t_\bullet)$, where we adopt $t_\bullet=10^{10}$ yr as the age of the SMBH (Gondolo & Silk 1999; Lacroix et al. 2014; Lacroix & Silk 2018). The power-law index γ is expected to be between 2.25 and 2.5 (Bøehm & Lavalle 2009), and in what follows we adopt $\gamma=7/3$.[11] Demanding continuation between the different profile segments, we find the spike radius, $R_{\rm spike}$, and the saturated radius of the DM density, due to self-annihilation, $R_{\rm sat}$ (shown in the bottom panel of Figure 2).

With the DM density profile at hand, we can now *roughly* estimate the mass of a self-gravitating clump. Using the results depicted in Figure 3, we find that particles that reach the inner region of the ergosphere spend about $f_{\rm whirl}\sim 0.01\%$ of their orbital time near the ergosphere. Thus, without loss of generality, we focus on these particles; as they develop their eccentricity over time, they swipe through the outer surface as well. Following Naoz & Silk (2014) we assume that about $f_{\rm acc}\sim 30\%$ of all particles can reach the ergosphere.[12] Note that since these particles, by definition, reached the ergosphere and eventually the event horizon, they will reach the closest approach that corresponds to the $f_{\rm whirl}$ value we adopt from Figure 3. Given different initial orbital configurations, different particles reach the required minimum pericenter at different times (e.g., Naoz & Silk 2014, Figure 9); since the eccentricity keeps on growing, the particles eventually are eaten by the SMBH. We scale this time dependency for different SMBH masses defining the fraction of particles with pericenter reaching the ergosphere inner surfaces as a function of time $f_{\rm EKL}(t)$; we can estimate the temporary clump mass as a function of time:

$$M_{\rm clump}\sim f_{\rm whirl}\times f_{\rm acc}\times f_{\rm EKL}(t)\times M_{\rm available,DM}, \quad (10)$$

where $M_{\rm available,DM}$ is the available mass of the DM particles estimated within the stable regime using the DM density profile from Equation (9). We show this mass as a function of time in the top panel of Figure 4. The mass is decreasing after about 100 Myr as particles either annihilate or are captured by the SMBH.

For annihilating DM particles, these high densities will undergo rapid annihilation. The annihilation timescale is

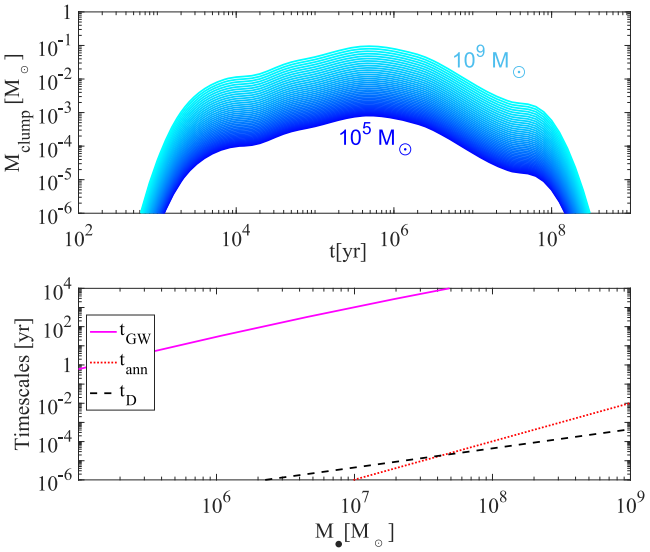

Figure 4. Top panel: we consider the mass of the self-gravitating clump as a function of time at $R_{\rm min}$, for a range of the primary SMBH masses from $10^9\,M_\odot$ (cyan, top) to $10^5\,M_\odot$, (blue, bottom). The time dependency is adopted from the Naoz & Silk (2014) dynamical simulations, where we assumed $e_{\rm p}=0.9$ and set $a_{\rm p}=R_{\rm Spike}$. The clump mass is estimated according to Equation (10). Bottom panel: the relevant timescales in the problem. We show the GW timescale, where we consider the maximum clump mass, and thus this is the shortest GW merger timescale. We also consider the dynamical timescale for a self-gravitating clump, Equation (5) (which is independent of annihilation processes). This timescale represents a significant change that a spherical clump undergoes due to its own gravity. Finally, we consider the annihilation timescale (Equation (11)), which is much shorter than the GW merger timescale.

estimated as

$$t_{\rm ann}\sim\frac{m_\chi}{\rho_{\rm SG}\langle\sigma v\rangle}, \quad (11)$$

shown as dotted lines in the bottom panel of Figure 4. We note that we use $\rho_{\rm SG}$ rather then $\rho_{\rm cl,max}$, because the former represents the minimum density at which the clump self-gravity will overcome the SMBH tidal forces, irrespective of self-annihilation. However, the strong gravitational field of the SMBH may affect the dynamics, and thus Equation (11) overestimates the annihilation timescale for masses below $M_{\bullet,\rm lim}$. As the clump self-annihilates, more particles can reach the ergosphere on high eccentric orbits via the EKL mechanism (as depicted in Figure 4, top panel), thus forming a new clump, and the process rejuvenates.

4. GW Emission Signal

The orbit of a self-gravitating clump will shrink due to GW emission. We estimate the merger timescale (Peters 1964), although we note that the clump is not a point mass; on the other hand, due to the EKL, it does not exhibit radial symmetry either. We adopt the maximum clump mass estimated from Figure 4, thus having a lower limit on the merger timescale between the clump and the SMBH (and the largest GW signal). As depicted in Figure 4, bottom panel, the merger timescale via GW emission is much longer than the annihilation timescale. Thus, while the clump undergoes self-annihilation, it emits a GW signal. In this example, the density around the SMBH will be replenished for about 10^8 yr, yielding continued GW and electromagnetic signals.

[10] The m–σ relation describes an observed correlation between the mass of the supermassive black hole at the centers of galaxies and the velocity dispersion σ of the galaxy bulge.

[11] We note that we have tested a larger value as well, which slightly changed the total clump mass but did not affect the overall, qualitative conclusion.

[12] Note that this value can be as low as 15% and as high as 50%. The former is a result of high eccentric particles that are captured by the massive SMBH perturber (Li et al. 2015), and the latter is a result of having the perturber SMBH grow in mass (Naoz & Silk 2014).

We note that the spin axis of the SMBH orientation can have an arbitrary direction compared to the SMBH binary orbital plane. The DM particles clump in the ergosphere in an asymmetric configuration, and follow highly eccentric geodesic trajectories through the ergosphere (Schnittman 2015). Thus, the actual waveform of such a signal is rather complicated and depends on the orbital dynamics of a test particle in a strong gravitational field (Will & Maitra 2017). We therefore estimate the dimensionless characteristic strain for a circular orbit, which represents the order of magnitude of the expected signal (Barausse et al. 2014). Moreover, most of the GW power is emitted near pericenter, so the circular orbit approximation indeed is a valid estimate (e.g., Enoki & Nagashima 2007; Tessmer & Gopakumar 2008).

The GW frequency f of a circular orbit is twice the orbital frequency, and the dimensionless characteristic strain is (Robson et al. 2019)

$$h_c(a, f) = 2h_0(a, f) f T_{\rm obs}, \tag{12}$$

where $T_{\rm obs}$ is the observation time window and $h_0(a, f)$ is defined as

$$h_0(a) = \sqrt{\frac{32}{5}} \frac{G^2}{c^4} \frac{M_\bullet M_{\rm clump}}{D_l a}, \tag{13}$$

where D_l is the luminosity distance and a is the semimajor axis of the two objects. Below we adopt $a = R_{\rm min}$. Note that while these calculations do not include the spin of the SMBH, they are an order of magnitude consistent with the latest implementation of the analytical model of extreme mass ratio inspirals that does include the spin of an SMBH for point mass inspiral (Chua & Gair 2015; Chua et al. 2017). We further emphasize that the strain calculation should be considered as strictly an order of magnitude, as orbits interior to the last stable orbit (such as in our case) cannot orbit on circular orbits.

Since the EKL mechanism yields an influx of DM particles on long timescales (e.g., Figure 4), as a clump become self-gravitating and self-annihilates, additional DM particles may reach high eccentricities. Thus, we can consider a long observational window with *LISA*. Figure 5 depicts the GW signal for two example sources observed for $T_{\rm obs} = 4$ yr. The first is located 2 Mpc away and the other located 0.02 Gpc from us. We consider a range of SMBH masses (from $10^5\,M_\odot$, to the right, to $10^9\,M_\odot$, to the left). As can be seen in the figure, *LISA* will be sensitive to a large range of the SMBH mass parameter space.

One may consider an observational window proportional to the annihilation timescale. This timescale covers a large range, from about a few days ($\sim$4 days for $10^9\,M_\odot$) to less than a minute for the low-mass SMBHs. This short timescale is still within the *LISA* sensitivity window. It is unclear how *LISA* will handle very short observational windows. However, as mentioned above, we expect a continuous formation of self-gravitating clumps of DM in the ergosphere, thus short timescales, which may be associated with burst-like signals, are less probable.

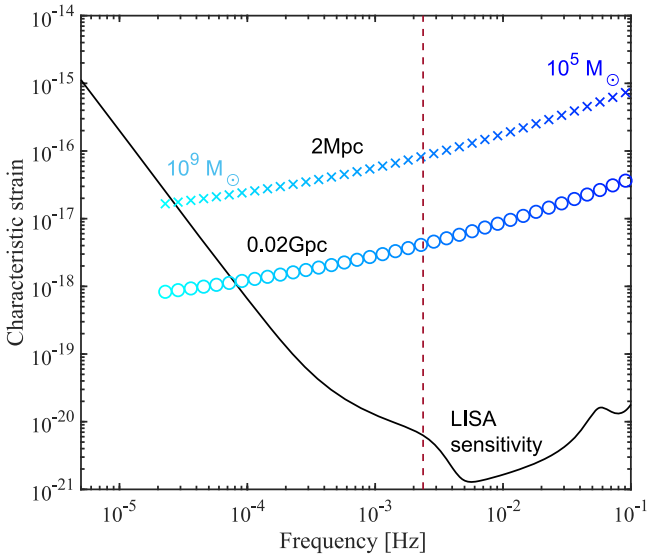

Figure 5. Examples for GW signal in the *LISA* band. We consider a 4 yr observational window for the source at 2 Mpc and 0.02 Gpc, top crosses and bottom circles, respectively. We show a range of SMBH masses from $10^9\,M_\odot$ (cyan, left) to $10^5\,M_\odot$, (blue, right). Overplotted is the *LISA* sensitivity curve (Robson et al. 2019). If DM self-annihilates, we find a limiting mass, $M_{\bullet,\rm lim}$ (corresponding to a maximum GW frequency), that can sustain the self-gravitating densities. We overplot the corresponding GW frequency of this mass (dashed red line). We remind the reader that the limiting clump mass, as well as the limiting GW frequency, depend on the DM mass and the annihilation cross-section; see Equation (7).

5. Discussion

We have shown that, thanks to the EKL mechanism in SMBH binaries, a self-gravitating DM clump may exist near the ergosphere of a spinning SMBH. DM may reach high eccentricities, spending considerable time there (see Figure 3), over long timescales allowing for replenishing the possibly self-annihilating DM particles (see Figure 4). The mass of the clump can be high enough to allow for a GW signal, detectable by *LISA* (as depicted in Figure 5). Our results suggest that this GW signal could be accompanied by a high-energy electromagnetic signal from DM self-annihilation processes, and locked in phase to the GW signal, similar to the chirps predicted from neutron star–BH mergers (Schnittman et al. 2018).

Note that if the DM does not self-annihilate into particles with detectable signatures, as is the case for gravitinos, we expect continuous formation of a massive clump around the SMBH. Unlike the assumptions made in Figure 4, where particles either self-annihilate or are captured by the SMBH, if all the particles survive, the mass of the clump may increase over time. Some of the DM particles may accrete onto the SMBH; however, the massive clump around the SMBH may result in, for example, gravitino decay products (Grefe 2012). Moreover, the GW signal in such a case may be even stronger, as the clump mass may increase. However, in the case with no electromagnetic counterpart we are unlikely to be able to distinguish between this GW merger and a stellar-mass extreme mass ratio inspiral. We note that we have assumed a gas-poor environment around SMBHs. Because the DM cusp dominates the density, and more so, as a clump becomes self-gravitating, we do not expect that interaction with the baryons will significantly alter the results.

SMBH binaries are a natural consequence of galaxy formation, consistent with observations (Barrows et al. 2018). We therefore expect that not only the torus-like DM distribution will be a generic outcome of SMBH binaries (Naoz & Silk 2014), but also will have a GW signal from self-gravitating DM that collects in the close vicinity of the SMBH.

If DM self-annihilates, we predict that the GW signal will also be accompanied by a high-energy signal.

S.N. and J.S. thank the UCLA Bhaumik Institute for Theoretical Physics for the hospitality that enabled the completion of this project. We thank the anonymous referees for useful comments that helped strengthen the Letter. We also thank Emanuele Berti, Bence Kocsis, and Bao-Minh Hoang for useful discussions. S.N. acknowledges the partial support of NASA grant No. 80NSSC19K0321, and also thanks Howard and Astrid Preston for their generous support. J.S. acknowledges discussions with Enrico Barausse. J.D.S. acknowledges support from NASA grant 17-TCAN17-0018.

ORCID iDs

Smadar Naoz https://orcid.org/0000-0002-9802-9279
Joseph Silk https://orcid.org/0000-0002-1566-8148
Jeremy D. Schnittman https://orcid.org/0000-0002-2942-8399

References

Ali-Haïmoud, Y., & Kamionkowski, M. 2017, PhRvD, 95, 043534
Ali-Haïmoud, Y., Kovetz, E. D., & Silk, J. 2016, PhRvD, 93, 043508
Antognini, J. M., Shappee, B. J., Thompson, T. A., & Amaro-Seoane, P. 2014, MNRAS, 439, 1079
Bansal, K., Taylor, G. B., Peck, A. B., Zavala, R. T., & Romani, R. W. 2017, ApJ, 843, 14
Barausse, E., Cardoso, V., & Pani, P. 2014, PhRvD, 89, 104059
Barrows, R. S., Comerford, J. M., & Greene, J. E. 2018, ApJ, 869, 154
Begelman, M. C., Blandford, R. D., & Rees, M. J. 1980, Natur, 287, 307
Berezinsky, V., Dokuchaev, V., Eroshenko, Y., Kachelrieß, M., & Solberg, M. A. 2010, PhRvD, 81, 103529
Berezinsky, V. S., Dokuchaev, V. I., & Eroshenko, Y. N. 2014, PhyU, 57, 1
Bertschinger, E. 1985, ApJS, 58, 39
Bianchi, S., Chiaberge, M., Piconcelli, E., Guainazzi, M., & Matt, G. 2008, MNRAS, 386, 105
Bøehm, C., & Lavalle, J. 2009, PhRvD, 79, 083505
Bogdanović, T., Eracleous, M., & Sigurdsson, S. 2009, ApJ, 697, 288
Boroson, T. A., & Lauer, T. R. 2009, Natur, 458, 53
Callegari, S., Mayer, L., Kazantzidis, S., et al. 2009, ApJL, 696, L89
Chiou, Y. S., Naoz, S., Burkhart, B., Marinacci, F., & Vogelsberger, M. 2019, ApJL, 878, L23
Chiou, Y. S., Naoz, S., Marinacci, F., & Vogelsberger, M. 2018, MNRAS, 481, 3108
Chua, A. J. K., & Gair, J. R. 2015, CQGra, 32, 232002
Chua, A. J. K., Moore, C. J., & Gair, J. R. 2017, PhRvD, 96, 044005
Comerford, J. M., Griffith, R. L., Gerke, B. F., et al. 2009, ApJL, 702, L82
Comerford, J. M., Nevin, R., Stemo, A., et al. 2018, ApJ, 867, 66
Deane, R. P., Paragi, Z., Jarvis, M. J., et al. 2014, Natur, 511, 57
Di Matteo, T., Springel, V., & Hernquist, L. 2005, Natur, 433, 604
Dotti, M., Montuori, C., Decarli, R., et al. 2009, MNRAS, 398, L73
Enoki, M., & Nagashima, M. 2007, PThPh, 117, 241
Eroshenko, Y. N. 2016, AstL, 42, 347
Ferrer, F., Medeiros da Rosa, A., & Will, C. M. 2017, PhRvD, 96, 083014
Gafton, E., & Rosswog, S. 2019, MNRAS, 487, 4790
Glampedakis, K., & Kennefick, D. 2002, PhRvD, 66, 044002
Gondolo, P., & Silk, J. 1999, PhRvL, 83, 1719
Green, P. J., Myers, A. D., Barkhouse, W. A., et al. 2010, ApJ, 710, 1578
Grefe, M. 2012, JPhCS, 375, 012035
Guo, H., Liu, X., Shen, Y., et al. 2019, MNRAS, 482, 3288
Hamers, A. S. 2018, MNRAS, 478, 620
Healy, J., Levin, J., & Shoemaker, D. 2009, PhRvL, 103, 131101
Hopkins, P. F., Hernquist, L., Cox, T. J., et al. 2006, ApJS, 163, 1
Jungman, G., Kamionkowski, M., & Griest, K. 1996, PhR, 267, 195
Katz, B., & Dong, S. 2012, arXiv:1211.4584
Kharb, P., Lal, D. V., & Merritt, D. 2017, NatAs, 1, 727
Kolb, E. W., & Tkachev, I. I. 1994, PhRvD, 50, 769
Komossa, S., Burwitz, V., Hasinger, G., et al. 2003, ApJL, 582, L15
Komossa, S., Zhou, H., & Lu, H. 2008, ApJL, 678, L81
Lacki, B. C., & Beacom, J. F. 2010, ApJL, 720, L67
Lacroix, T., BÅ'hm, C., & Silk, J. 2014, PhRvD, 89, 063534
Lacroix, T., & Silk, J. 2018, ApJL, 853, L16
Li, G., Naoz, S., Holman, M., & Loeb, A. 2014a, ApJ, 791, 86
Li, G., Naoz, S., Kocsis, B., & Loeb, A. 2014b, ApJ, 785, 116
Li, G., Naoz, S., Kocsis, B., & Loeb, A. 2015, MNRAS, 451, 1341
Liu, J., Eracleous, M., & Halpern, J. P. 2016, ApJ, 817, 42
Liu, X., Greene, J. E., Shen, Y., & Strauss, M. A. 2010, ApJL, 715, L30
Luo, L., Katz, B., & Dong, S. 2016, MNRAS, 458, 3060
Milosavljević, M., & Merritt, D. 2001, ApJ, 563, 34
Misner, C. W., Thorne, K. S., & Wheeler, J. A. 1973, Gravitation (San Francisco, CA: W. H. Freeman)
Naoz, S. 2016, ARA&A, 54, 441
Naoz, S., Farr, W. M., & Rasio, F. A. 2012, ApJL, 754, L36
Naoz, S., Kocsis, B., Loeb, A., & Yunes, N. 2013, ApJ, 773, 187
Naoz, S., & Narayan, R. 2014, ApJL, 791, L8
Naoz, S., & Silk, J. 2014, ApJ, 795, 102
Navarro, J. F., Frenk, C. S., & White, S. D. M. 1996, ApJ, 462, 563
Pesce, D. W., Braatz, J. A., Condon, J. J., & Greene, J. E. 2018, ApJ, 863, 149
Peters, P. C. 1964, PhRv, 136, 1224
Popa, C., Naoz, S., Marinacci, F., & Vogelsberger, M. 2016, MNRAS, 460, 1625
Ricotti, M. 2009, MNRAS, 392, L45
Robertson, B., Bullock, J. S., Cox, T. J., et al. 2006, ApJ, 645, 986
Robson, T., Cornish, N., & Liu, C. 2019, CQGra, 36, 105011
Rodriguez, C., Taylor, G. B., Zavala, R. T., et al. 2006, ApJ, 646, 49
Runnoe, J. C., Eracleous, M., Pennell, A., et al. 2017, MNRAS, 468, 1683
Schnittman, J. D. 2015, ApJ, 806, 264
Schnittman, J. D., Dal Canton, T., Camp, J., Tsang, D., & Kelly, B. J. 2018, ApJ, 853, 123
Silk, J., & Stebbins, A. 1993, ApJ, 411, 439
Sillanpaa, A., Haarala, S., Valtonen, M. J., Sundelius, B., & Byrd, G. G. 1988, ApJ, 325, 628
Smith, K. L., Shields, G. A., Bonning, E. W., et al. 2010, ApJ, 716, 866
Starobinskij, A. A. 1992, JETPL, 55, 489
Tessmer, M., & Gopakumar, A. 2008, arXiv:0812.0549
Tremaine, S., Gebhardt, K., Bender, R., et al. 2002, ApJ, 574, 740
Tsupko, O. Y. 2014, PhRvD, 89, 084075
Will, C. M., & Maitra, M. 2017, PhRvD, 95, 064003
Yu, Q. 2002, MNRAS, 331, 935